



Deformation within a strike-slip fault network at Westward Ho!, Devon U.K.: Domino vs conjugate faulting

Casey W. Nixon^{a,*}, David J. Sanderson^{a,b,c}, Jonathan M. Bull^a

^a School of Ocean and Earth Science, University of Southampton, National Oceanography Centre Southampton, SO14 3ZH, UK

^b School of Civil Engineering and the Environment, University of Southampton, SO17 1BJ, UK

^c EPT, BP Exploration Operating Company Limited, Chertsey Road, Sunbury on Thames, TW16 7BP, UK

ARTICLE INFO

Article history:

Received 23 August 2010

Received in revised form

7 March 2011

Accepted 11 March 2011

Available online 21 March 2011

Keywords:

Fault networks

Domino faulting

Conjugate faulting

Strike-slip

Displacement

Strain

ABSTRACT

A system of NE trending left-lateral faults and NW-trending right-lateral faults at Westward Ho! (north Devon, U.K.) cut steeply dipping ($\sim 60^\circ$) strata. Faults were accurately mapped in the field and from aerial photography, and lateral separations of marker beds measured along the fault traces. These data are used to examine the displacements within the network of interacting faults and to calculate variations in the density and relative proportions of the fault sets. The displacements are also used in a tensor analysis of the strain and, together with block rotations, used to restore the deformation. The results show a range of heterogeneity within the fault network, both in terms of the fault patterns and strain. Some sub areas show a dominance of one fault set, with regularly spaced larger displacements, separating relatively weakly deformed blocks with smaller antithetic faults. Within these areas up to 20° rotation of the faults and bedding produces a domino style deformation that accommodates up to $\sim 15\%$ extension. The domino regions are separated by areas of conjugate faulting, in which both sets of faults are equally developed and have similar displacement ranges. Conjugate areas have little or no rotation of the bedding and generally lower strains than domino regions.

© 2011 Elsevier Ltd. All rights reserved.

1. Introduction

The major aim of this paper is to characterise the deformation and kinematic behaviour within a strike-slip fault network and demonstrate the applicability to other fault networks. The geometry, connectivity, displacement distribution, role of different fault sets and strain distribution are important to understanding fault networks. These features are important for controlling the behaviour of the rock mass. For example, fault networks provide pathways for fluid flow that are important in the generation, exploration and production of hydrocarbons, groundwater and mineral deposits, and in understanding the distribution of displacement and earthquakes in active systems (e.g. King, 1986; Sibson, 1989; Taylor et al., 2004).

Much work has been done to determine the movement and formation of individual faults (Muraoka and Kamata, 1983; Barnett et al., 1987; Walsh and Watterson, 1987, 1988; Nicol et al., 1996; Kim et al., 2001) and interacting fault segments (Peacock, 1991; Peacock and Sanderson, 1994, 1995; Cartwright et al., 1995; Childs et al., 1995; Huggins et al., 1995; Taylor et al., 2004). Such studies have

increased our understanding of the growth and evolution of individual fault zones (Cox and Scholz, 1988), particularly for strike-slip faults (Aydin and Schultz, 1990; Peacock, 1991; Peacock and Sanderson, 1995; Du and Aydin, 1995; Kim et al., 2003). Single sets of faults may become organised to accommodate crustal deformation, as in the case of domino faulting and associated block rotations (Luyendyk et al., 1980; Nur et al., 1986; Axen, 1988; Peacock et al., 1998) or more commonly two or more fault sets may interact to produce a fault network. The simplest example of this is a pair of conjugate faults (e.g. Freund, 1974; Nicol et al., 1995; Zhao and Johnson, 1991; Kelly et al., 1998).

This paper seeks to extend and develop such studies to large fault networks, within which deformation may be distributed with varying degrees of heterogeneity as a result of the interaction and localization of displacement and strain (e.g. Zhang and Sanderson, 2001). It describes and identifies the characteristics and behaviour on a mesoscale strike-slip fault network at Westward Ho!, north Devon. Furthermore, it assesses the variation in geometry and kinematics that exist within the network, focussing on the way that the faults interact with one another, the spatial variations in their geometry and the strain that is produced.

Strike-slip systems are very suitable for such analysis since most of the significant variation is presented in map-view. Hence the

* Corresponding author.

E-mail address: c.w.nixon@noc.soton.ac.uk (C.W. Nixon).

requirements for this study were a well-exposed surface with many faults and a detailed (and steeply dipping) stratigraphy that would allow accurate determination of fault displacement throughout the network. The wave-cut platform at Westward Ho!, north Devon, provides such conditions.

2. Geological setting

The strike-slip faults at Westward Ho! cut Upper Carboniferous stratigraphy comprising repeated, coarsening upwards cycles of mudstones, siltstones and sandstones, originally deposited in a deltaic environment (Elliott, 1976). These cycles are divided into two units (Fig. 1): the Westward Ho! Formation (~400 m) and the Bideford Group (~800 m) (Walker, 1970; Elliott, 1976; Higgs et al., 1990). This detailed stratigraphy provides a basis for the accurate determination of displacement along the faults.

WNW-trending upright folds are observed in the Bideford Group and formed during Variscan deformation (Sanderson, 1984) that inverted the basin at the end of the Carboniferous period. The strike-slip faults are divided into NE trending left-lateral faults and NW-trending right-lateral faults, implying an N–S directed maximum horizontal principal stress during deformation.

Much of SW Britain was affected by late Variscan NW-SE strike-slip faulting (Dearman, 1963) that cross-cuts earlier folds and thrusts. This deformation was part of a late Variscan right-lateral shear zone that transected southern Europe during the Late Palaeozoic (Arthaud and Matte, 1977; Badham, 1982), as a result of right-lateral transpression due to oblique NW-SE convergence between the African and European plates (Coward and McClay, 1983; Sanderson, 1984; Barnes and Andrews, 1986; Holdsworth, 1989).

The strike-slip faults at Westward Ho! clearly post-date the Variscan folds and, hence, are either related to this late Variscan event or to later Cretaceous-Tertiary N–S shortening (Lake and Karner, 1987; Chadwick, 1993; Peacock and Sanderson, 1998). The precise age or cause of the faults in the area is not required for this study, because the faults do not appear to show signs of multiphase movement or reactivation. What is important is that the faults are strike-slip in nature and, hence, their displacement can be characterised by measuring the mapped offsets of the known stratigraphy.

The map (Fig. 1) shows two dominant sets of faults cutting steeply dipping (>60°) beds. The faults are interpreted as forming a strike-slip fault network on the basis of:

- 1) In map-view, they form two sets with relatively straight traces at about 60–70° to each other (Fig. 2);
- 2) The NW–SE set consistently produces right-lateral separations of marker beds, whereas the NE–SW trending set has consistent left-lateral separations (Figs. 3 and 4);
- 3) Both sets of faults are sub-vertical and their intersection is steeply plunging (Fig. 2b);
- 4) Both sets have sub-horizontal slickenside lineations (Fig. 2b);
- 5) Occasional fold hinges are offset laterally by the faults and have both limbs offset with the same separation.

Both fault sets extend layering sub-parallel to bedding strike (~E–W). The possibility that they could have developed as normal faults prior to the steepening of the beds can be dismissed because the faults cross-cut the folds and have similar geometry and separations on opposite limbs (point 5 above).

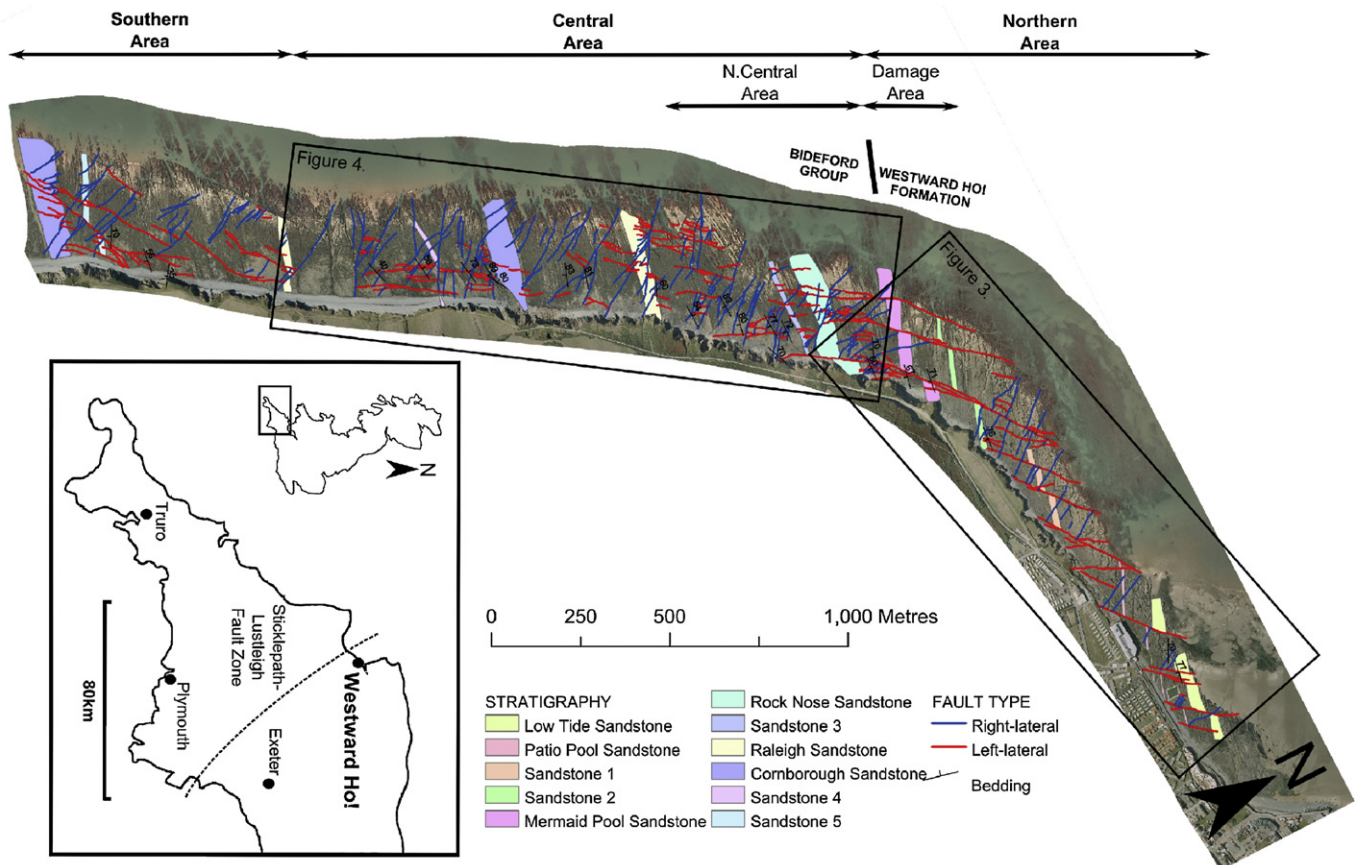


Fig. 1. Interpreted aerial photograph of the wave-cut platform at Westward Ho! showing the main sandstone units. The northern area corresponds to Fig. 3 and the central area to Fig. 4. Inset is a location map of the area. Image/Data courtesy of the Channel Coastal Observatory.

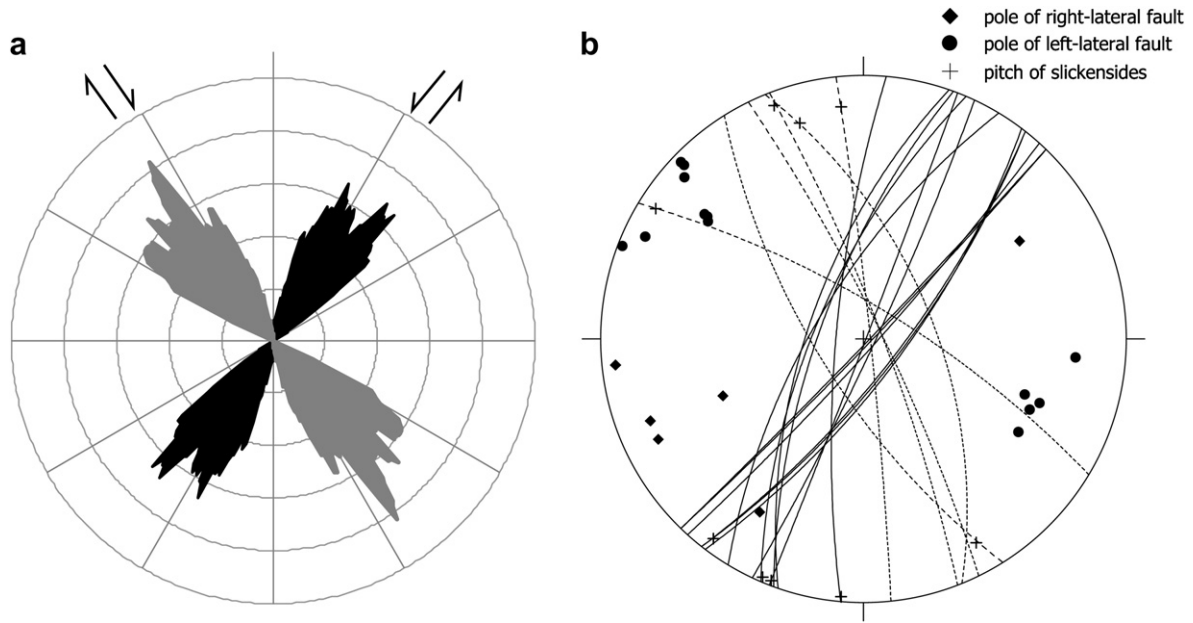


Fig. 2. a) Length-weighted rose diagram of the study area with grey representing right-lateral faults and black for left-lateral faults. b) Equal-area stereographic projection of fault data throughout the area. Dotted lines represent right-lateral faults and solid lines represent left-lateral faults.

3. Methodology

3.1. Mapping

The fault network at Westward Ho! is continuously exposed along a 4 km-long wave-cut platform, with a width of 200–400 m (Fig. 1). Digital aerial photography of the wave-cut platform was acquired at low tide in 2006 and made available courtesy of the Channel Coast Observatory. The images have a pixel resolution of

0.1 m (equivalent to a 1:5000 scale film) and are orthorectified. These aerial images were used to provide excellent base maps for detailed mapping, and to expand the field mapping to cover the entire coastal strip.

Marker beds on either side of faults were correlated and their lateral separations measured. The maps were integrated with previous mapping by Walker (1970) and Higgs et al. (1990). Structural data were also collected, including bedding and fault orientations, as well as slickenside measurements where possible.

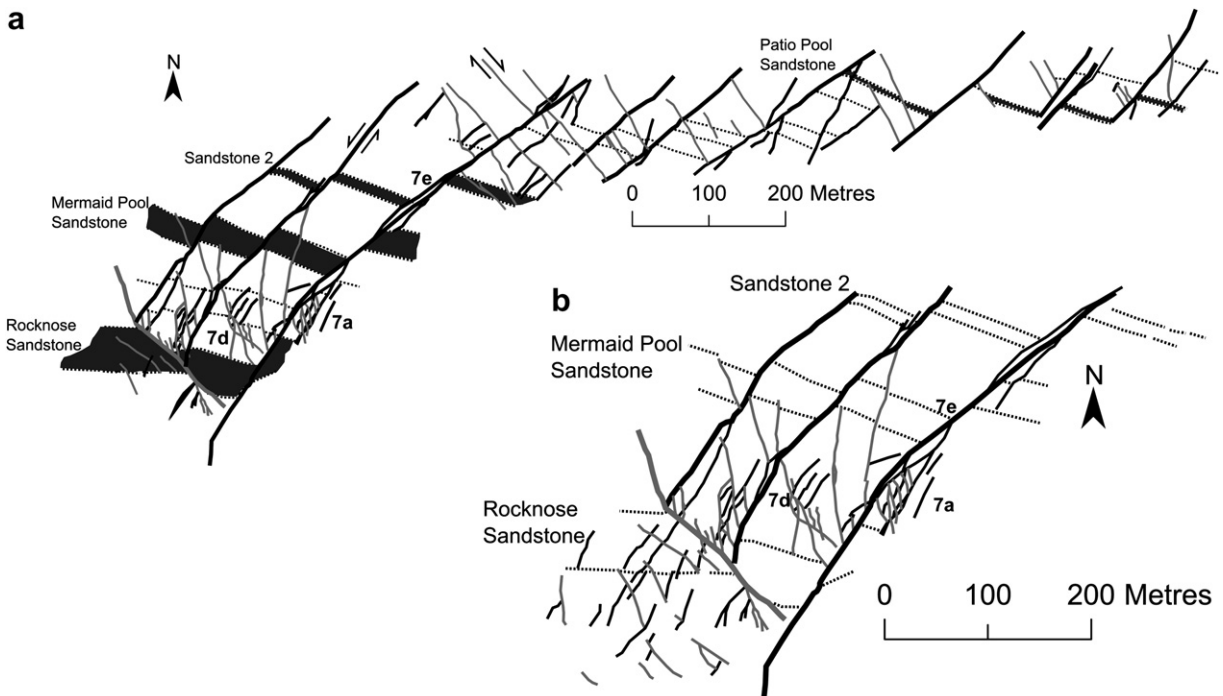


Fig. 3. a) Map of the northern area in Fig. 1, which shows the dominance and slight rotation of left-lateral faults. b) An enlarged fault map of a damage zone at the southern limits of the northern area (Fig. 3a). The location of the D-X plots in Fig. 7a, d and e are indicated. Solid lines represent faults with grey and black for right- and left-lateral faults, respectively.

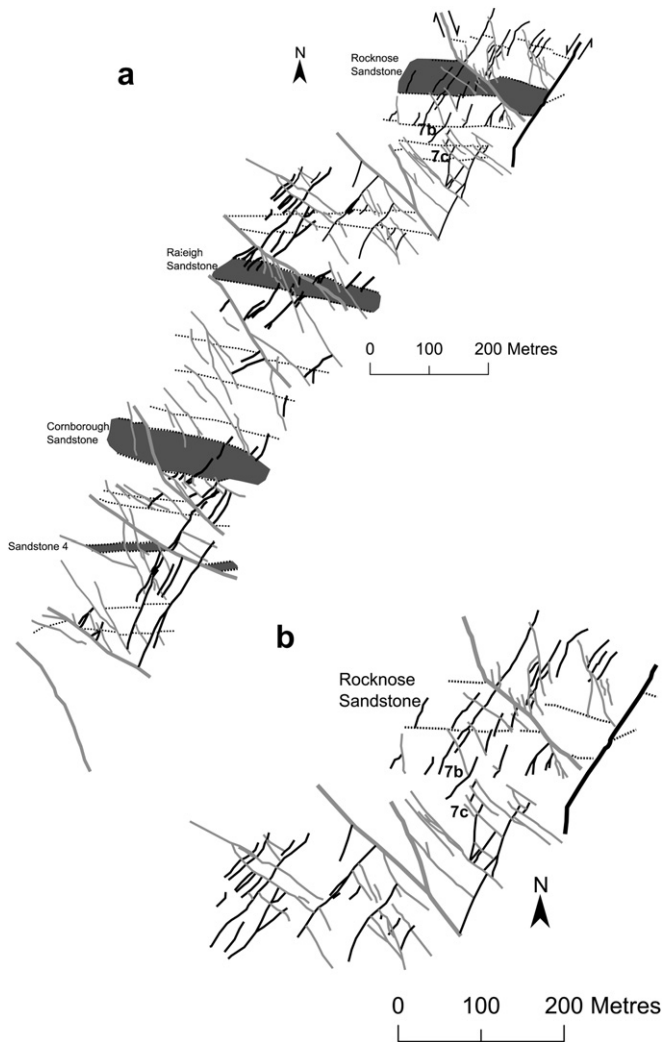


Fig. 4. a) Map of the central area in Fig. 1, which shows the dominance of right-lateral faults. b) An enlarged fault map of the north central area showing a greater concentration of smaller magnitude faults of both fault sets. The location of the D-X plots in Fig. 7b and c are indicated. Solid lines represent faults with grey and black as right- and left-lateral faults, respectively.

3.2. Displacement analysis

The orthorectified aerial images were imported into ArcGIS with all the field data and interpreted marker beds. The cut-offs of marker beds were digitized along most faults, allowing the calculation of separations at locations along fault traces. Data from ArcGIS were exported to spreadsheets for further analysis and display ($d-x$ plots, rose diagrams, etc.).

Lateral separations of beds on the sub-horizontal wave-cut platform approximate the strike-slip displacement of the faults. In the field, direct measurement of separation was done using a 30 m tape. Measurements of lateral separations also used the measuring tool in ArcGIS. Comparison of these two approaches showed excellent agreement and separations are considered to have errors of <0.5 m for large faults, with direct field measurement of separations on small faults being accurate to ~10 mm.

Given that displacement and fault orientation are available for many positions along faults, we displayed the information in four ways:

1) *Displacement–distance ($d-x$) plots* were produced for selected faults, where the distance (x) may be the length along the fault

trace or the projection of this length along some chosen direction. The latter type of plot is mainly used to look at the interactions of NW and NE trending faults and, hence, the N–S direction is a convenient common reference. Where faults intersect each other, displacement profiles were produced for each interacting fault branch and extrapolated to the intersection point. Consequently, no displacement was allocated to the intersection point because it represents an abrupt change in displacement from one fault branch to another.

- 2) *Displacement-orientation plots*, which are simply scatter-plots of displacement against fault strike for each fault segment, are used to indicate differences in the displacement characteristics for the different fault sets.
- 3) *Length-weighted rose diagrams* were obtained by calculating the total trace length within varying orientation bins. In general a 15° class interval was used centred on a 1° step around the circle. These plots are mainly to examine the variation in frequency and orientation of the fault sets in different sub areas.
- 4) *(Length × displacement) weighted rose diagrams* are similar to length-weighted rose diagrams, except that the distribution of the product of trace length × displacement is plotted against orientation. These plots therefore indicate the dominant displacements on the different fault sets throughout the network.

3.3. Strain determination

Strain analysis was conducted using a technique based on the method developed by Peacock and Sanderson (1993). This approach involves the calculation of a displacement tensor D_{ij} , that is formed from the cross-product of the unit vector normal to the fault plane, (n) and the displacement direction within the fault plane, ($s u$), where u is a unit vector in the slip direction and s is the displacement on the fault. Peacock and Sanderson (1993) applied this approach to N faults sampled along a line of length L , using a weighting factor (w) to correct for the orientation bias of such samples, where $D_{ij} = ws(n \times u)$. The Lagrangian strain tensor is E_{ij} , is given by:

$$E_{ij} = N/L \sum [(D_{ij} + D_{ji})/2] \quad (1)$$

The same approach is valid for sampling on a plane. The weight (w) is determined from the angle between the fault normal and the plane. As the strike-slip faults are sub-vertical, both the fault normal and displacement vector are sub-horizontal and, hence, the weighting factor can be ignored (i.e. $w \rightarrow 1$).

If the fault trace strikes at an angle θ to north then:

$$n = (-\sin\theta, \cos\theta) \text{ and } u = (\cos\theta, \sin\theta) \quad (2)$$

and,

$$\begin{aligned} D_{ij} &= \sum s \begin{pmatrix} n_1 u_1 & n_1 u_2 \\ n_2 u_1 & n_2 u_2 \end{pmatrix} \\ &= \sum s \begin{pmatrix} -\sin\theta \cos\theta & -\sin^2\theta \\ \cos^2\theta & \cos\theta \sin\theta \end{pmatrix} \end{aligned} \quad (3)$$

where s is +ve for left-lateral and –ve for right-lateral faults. The term n/L in equation (1) represents the fault density and is replaced in the planar sample by $\Sigma(\text{tracelength})/\text{area}$ ($\Sigma t/A$), the 2-D equivalent of the fault density. Thus the Lagrangian strain tensor is given by:

$$E_{ij} = 1/A \sum [(tD_{ij} + D_{ji})/2] \quad (4)$$

The eigenvectors and eigenvalues of the strain tensor provide estimates of the orientation and magnitude of the principal strains.

4. Fault network characteristics

4.1. Spatial distribution and magnitude variation of fault sets

The two sets of strike-slip faults vary in their relative abundance throughout the Westward Ho! area (Figs. 1, 3 and 4). The northern area (Fig. 3) is dominated by a series of long left-lateral faults, whereas the adjacent region to the south (Fig. 4b) has approximately equal distributions of left- and right-lateral faults. By contrast, in the central part of the study area (Fig. 4a) large right-lateral faults are dominant. This variation is clearly seen in the rose diagrams of the trace length distributions that show a dominance of left-lateral faults in the northern area (Fig. 5a) and right-lateral faults in the south-central area (Fig. 5c) with a region of more equal representation of both sets in the centre (Fig. 5b).

Fault displacements may be as large as 80 m, but 79% of the overall fault trace length has displacements less than 10 m. The distribution of fault displacements varies (Fig. 6). In the left-lateral dominated area in the north, faults with displacements >10 m form about half the mapped trace length and all are left-lateral (Fig. 6a). In contrast, in the north central area (Fig. 4b) only 10% of the trace length is formed from large (>10 m) displacement faults, which include both left- and right-lateral sets.

The (length × displacement) weighted rose diagrams (Fig. 5) further emphasize that the dominant fault set changes across the area. The north central area still has equal proportions of both fault sets (Fig. 5e), whereas the areas to the north and south have a dominance of left (Fig. 5d) and right (Fig. 5f) lateral displacement, respectively.

The left-lateral dominated areas in the north (Fig. 3) and at the southern limits of the study area are characterised by large magnitude (10–80 m) left-lateral faults, and large magnitude right-lateral faults characterise the right-lateral dominated central area (Fig. 4a). The large left-lateral faults are more closely spaced (75–100 m) than their right-lateral counterparts (100–200 m) and have smaller displacements than the largest right-lateral faults.

4.2. Displacement profiles and interaction of fault sets

Isolated faults are relatively uncommon and tend to be small faults with a simple pattern of displacement that increases from zero at the tips to a maximum value, usually near the centre of the fault trace (Fig. 7a). This pattern has been widely described before (e.g., Barnett et al., 1987).

Y- or T- shaped intersections are where a fault abuts against a fault of the other set (e.g., Fig. 7b). Displacement changes abruptly on AB at the intersection (C), which corresponds to a similar change on CD. Thus, both faults show similar displacement patterns as they approach their intersection point, such that the displacements on both faults almost cancel out one another. Another important feature of many Y-shaped intersections is that the displacement on the abutting fault (CD) increases away from the intersection (c.f. splays discussed below).

X-shaped intersections result when two faults cross-cut one another. They are much less frequently than Y-intersections, and are commonly small-displacement (<10 m) faults (e.g., Fig. 7c). For example, a left-lateral fault (AB) and a right-lateral fault (CD) have displacements of 4 m and 8 m at points A and C, respectively, with

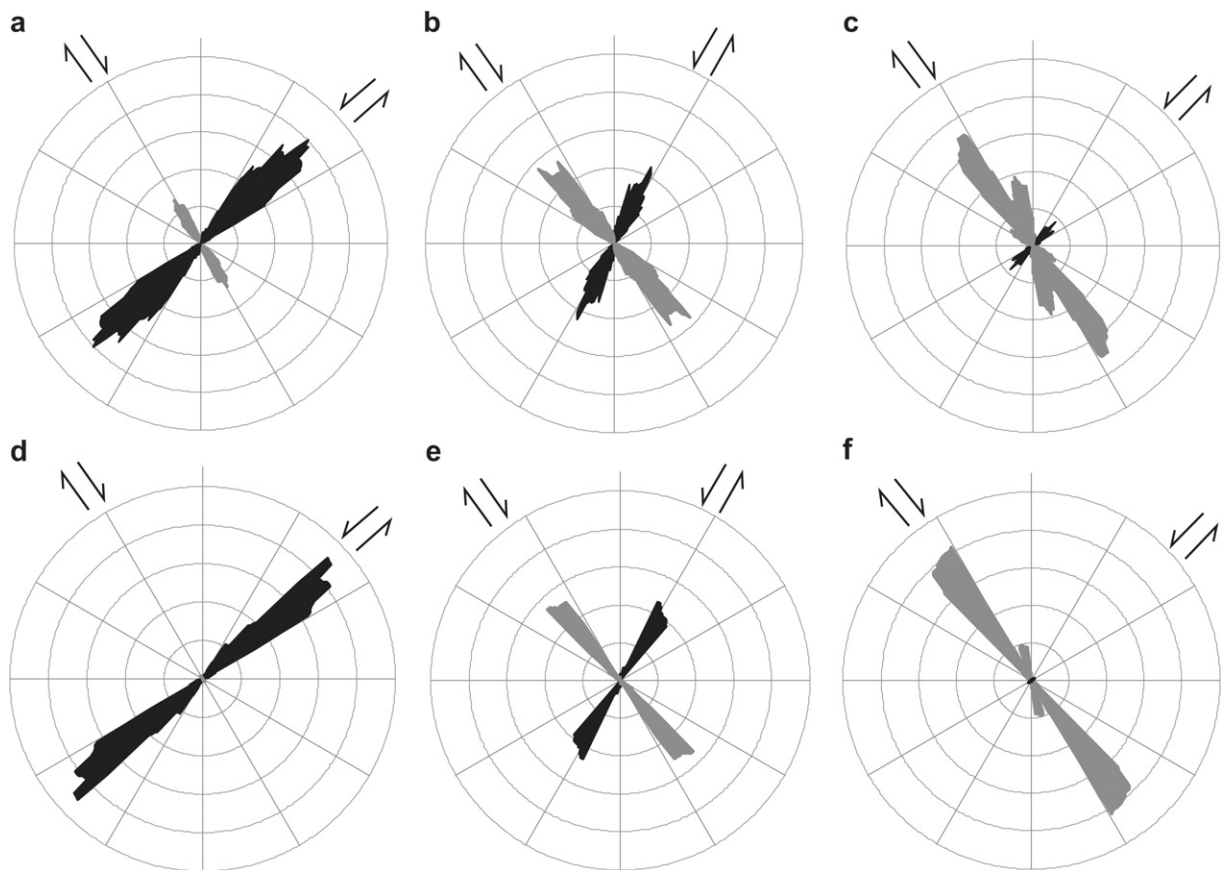


Fig. 5. Length-weighted rose diagrams for: a) the northern area; b) the north central area; c) the central area. (Length × displacement) weighted rose diagrams for: d) the northern area; e) the north central area; f) the central area with a dominance of right-lateral faults. Note the change in dominance from north to south. Grey represents right-lateral faults and black represents left-lateral faults.

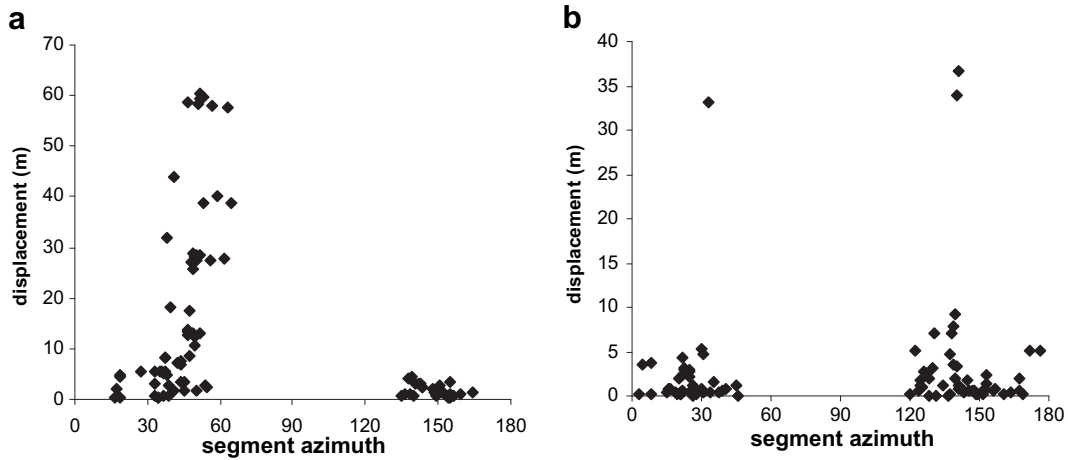


Fig. 6. Plot of displacement against azimuth for: a) the northern area; b) the north central area.

tips at B and D (Fig. 7c). At the intersection point, the displacements decrease to about 2 m on both faults at steps of ~1 m. Assuming that these faults were propagating towards their tips, much of the displacement was possibly achieved prior to their intersection. The similarity in the stepping of the displacement and the lack of offset

suggests that one fault is not simply displacing the other. Such intersections cannot be reconstructed by the movement of rigid blocks and must involve significant internal deformation of the fault blocks. They may form due to sequential movement of the fault sets (Freund, 1974; Ramsay and Huber, 1987; Zhao and

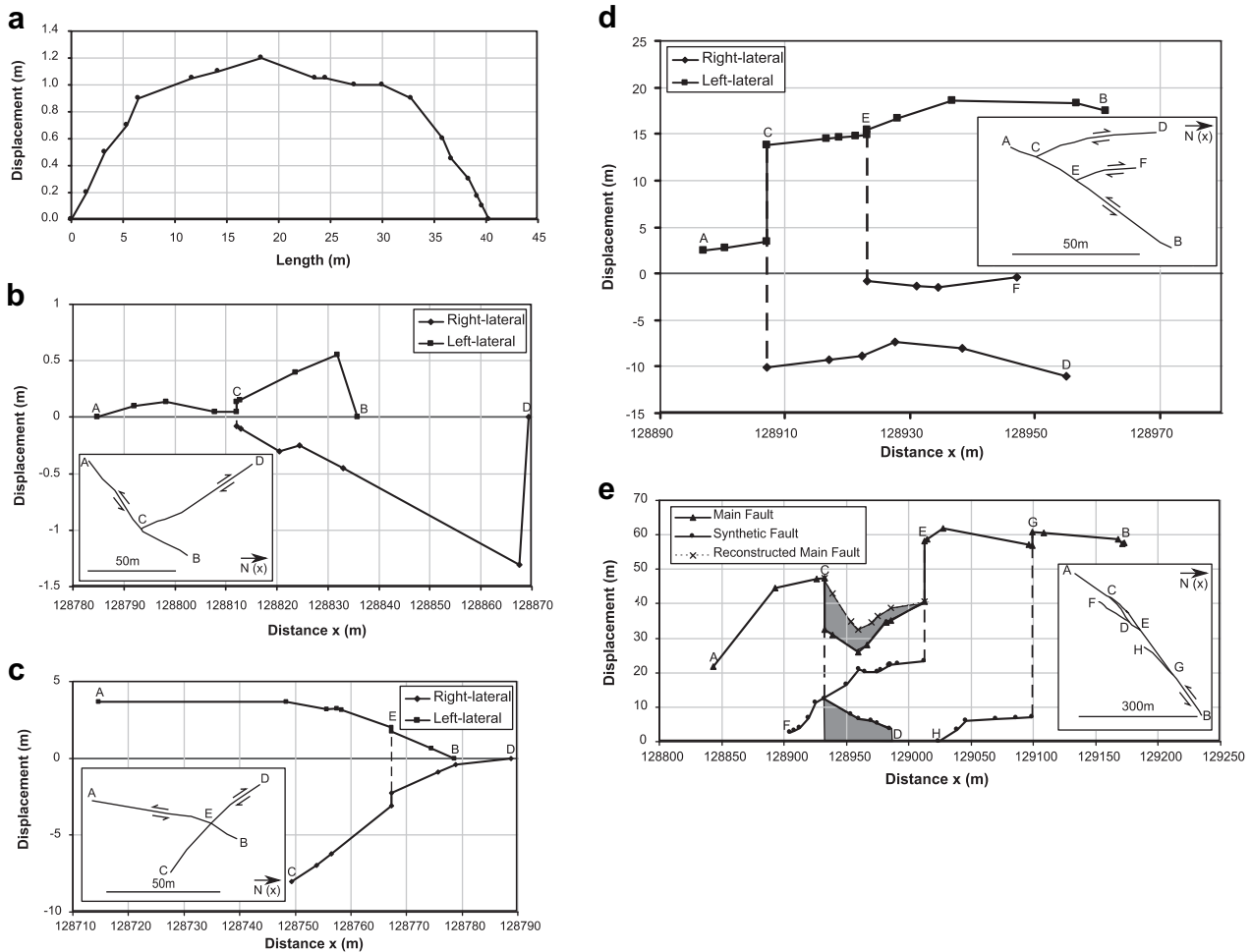


Fig. 7. Plots of displacement against distance for different fault interactions in which left- and right-lateral displacements are plotted as +ve and -ve, respectively: a) an isolated fault; b) Y-shaped intersection; c) X-shaped intersection; d) antithetic fault interactions; e) synthetic fault interaction with a damage lens, and a reconstructed profile for the main fault without the lens is also plotted. For each d-x plot an inset shows the plan-view geometry of the fault intersection.

Johnson, 1991) or simultaneous movement of the two fault sets (Horsfield, 1980; Nicol et al., 1995). At Westward Ho!, these X-intersections are usually developed in mud-rich parts of the sequence.

All faults that abut or cross-cut each other produce Y- or X-shaped intersections, respectively. Still, two additional intersection geometries are:

Antithetic fault interactions result when smaller displacement faults abut (or occasionally cross-cut) larger displacement faults with the opposite motion sense, producing a series of Y- (and occasionally X-) shaped intersections along the major fault. They generally produce small steps in the d-x profiles of the dominant faults. For example, the left-lateral fault (AB) in Fig. 7d has a displacement (18 m) with two interacting antithetic faults (CD - 10 m and EF - 2 m). Both antithetic faults maintain a near constant displacement approaching the main fault and at the intersection. At the intersections, the 10 m and 1 m displacements on CD and EF produce corresponding changes in the displacement on fault AB. A series of antithetic faults on the same wall of the dominant fault created stepped displacement changes and characteristically is a geometry by which faults reduce displacement towards their tip (e.g., Fig. 7d).

Synthetic faults are where a major fault branches, producing a series of Y-shaped intersections and lenses. The splays generally have smaller displacements with the same sense of motion, and occur at a small angle (generally < 30°) to the major fault. Splays that rejoin the main fault produce lenses.

Fig. 7e shows a left-lateral fault with a displacement of ~60 m that has a series of splays (at E and G) and lenses (between C and D). The total displacement on the main fault is determined by combining the displacements C to D with that on the main trace between C and E. This determination produces a displacement profile with two main steps at E and G. A simple splay occurs at G with a ~6 m step in displacement onto the splay, that branches from the main fault and extends for ~75 m to a tip at H. Another splay occurs at E with a ~20 m step in displacement onto the splay, that branches from the main fault and extends for ~200 m to a tip at F. Note that in both cases, the maximum displacement for the splay is at the intersection (E and G) with the main fault.

The development and spatial distribution of these different interactions varies throughout the study area. The north central area (Fig. 4b) has many Y- and X-shaped intersections of

small-magnitude faults in areas between large magnitude faults. In contrast, the northern area (Fig. 3a) has a more organised arrangement of large left-lateral faults that have intersections with smaller interacting antithetic faults (and some synthetic faults). These synthetic and antithetic faults are more concentrated in the damage area (Fig. 3b) between these two regions.

4.3. Strain

The Lagrangian strain tensor, determined from the fault displacements, shows a variation in the maximum extension from <5% to >15% (Fig. 8, Table 1). The largest extension (15.5%) is in the northern area, with 10.4% in the damage area and 5.3% in the north central area. The strains increase to the south (Fig. 8b). The strain in the northern area is accommodated by the block rotation and larger displacement along the left-lateral faults. It is about three times greater than in the north central region, which has approximately equal numbers of left- and right-lateral faults with negligible block rotation.

An overall E-W (N093°E) extension is present in the north central area of conjugate faults (Fig. 4b), changing to ENE-WSW (N068°E) in the northern area. In the central area, the trend is WNW-ESE (N114°E) where right-lateral faults dominate (Fig. 4a). Furthermore, the changes in extension direction coincide with changes in percentage extension (Fig. 8). This change supports the idea that greater rotational strains are developed where one fault set dominates in different areas of the fault network.

A graph of the % maximum extension against N-S distance (Fig. 8b) illustrates a progressive change in strain between the northern, central and southern areas. The extension in an E-W direction is ~5% in the northern area and is, hence, compatible with the E-W extensions in the conjugate region to the south such that no discontinuities are required at subarea boundaries.

Strain restoration (Fig. 9) was performed by dividing a region into blocks of stratigraphy bounded by the main faults. The blocks were rotated until the stratigraphic bedding was orientated approximately E-W with fault displacements removed. This procedure produced a restoration with only minor gaps and overlaps (Fig. 9). The north central area was restored by removing the displacements on the two sets of faults without rotation (Fig. 9a). In contrast, the northern area, which is dominated by left-lateral faults, shows a pronounced left-lateral shear accompanied by N-S

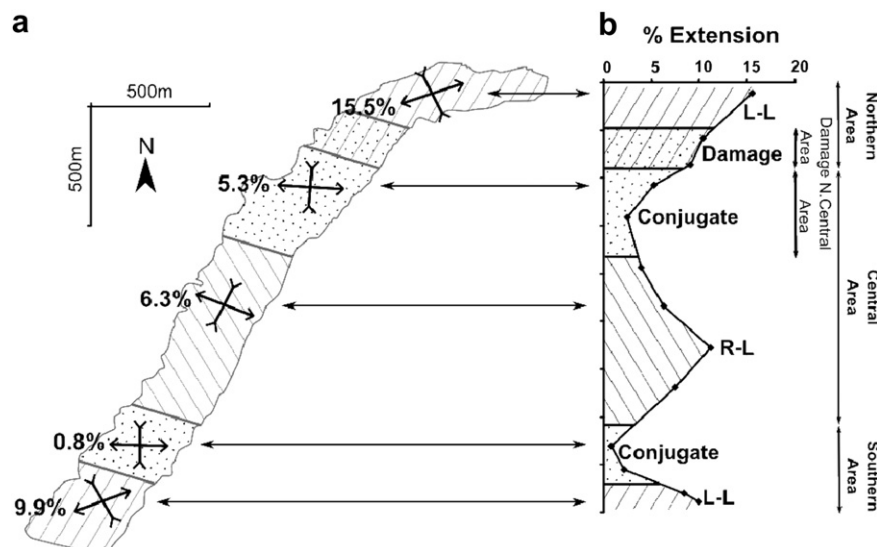


Fig. 8. a) Diagram showing the orientations of the principal horizontal extensions for different sub areas. b) Graph of % extension plotted against distance.

Table 1
Structural characteristics of mapped areas (Fig. 1) at Westward Ho!

	Northern area	Damage area	N. Central area	Central area
	Domino (left-lateral)		Conjugate	Domino (right-lateral)
Fault density (km^{-1})	11	39	28	19
%extension	15.5	10.4	5.3	6.3
Direction of maximum extension (θ)	N068°E	N073°E	N093°E	N114°E

shortening or left-lateral transpression that is accommodated by large-displacements on the left-lateral faults and clockwise rotation of the intervening blocks (Fig. 9b). This is consistent with the compatibility of deformation between the regions. Thus, the larger strains in the northern area are accommodated by the increased rotation.

The fault densities of the four sub areas were also calculated (Table 1), where a density of 25 km^{-1} means that 25 km of fault trace length is present in each square km of wave-cut platform. Again, fault densities vary between areas and even between right-lateral and left-lateral dominated areas.

5. Domino v conjugate faulting

Variation in fault style on the wave-cut platform at Westward Ho! can be interpreted with reference to conjugate and domino models. Conjugate systems comprise similar numbers of the two intersecting sets of faults with their opposite displacement senses, which accommodate pure shear bulk deformation with little rotation of bedding. The maximum and minimum principal stress directions (σ_1 and σ_3) bisect the angle between the two fault sets, with σ_1 as the acute angle ($\sim 60^\circ$) bisector (Fig. 10). Domino faulting, on the other hand, consists of mainly one fault set, producing fault bounded blocks which rotated during deformation (e.g. Axen, 1988) (Fig. 10). Fault blocks may have internal deformation due to the presence of smaller magnitude faults. The distribution and arrangement of small faults within a fault block can sometimes counteract the rotation of the fault block (Peacock et al., 1998).

5.1. Conjugate area

An area of conjugate faults is found in the north central area and separates the right-lateral and left-lateral dominant areas (Fig. 8).

In this area, both left-lateral and right-lateral faults are developed to a more-or-less equal degree (Fig. 5b and e). The maximum weighted azimuth for the fault sets are N320°E for right-lateral faults and N030°E for left-lateral faults with a bisector at N355°E, which is assumed to approximate the maximum horizontal compressive stress direction during deformation. The area consists dominantly of small-displacement ($< 10 \text{ m}$) faults that compose 90% of the trace fault length (Fig. 6b). The fault density is 28 km^{-1} and the faults produce 5.30% extension in an E–W direction (Table 1).

Small-displacement faults typically form conjugate Y- and X-shaped intersections, which have similar displacements and experience related changes in displacement at intersection points (Fig. 7b and c). Within this region, the overall strike of bedding is approximately E–W, and is only locally deflected adjacent to both sets of faults. Restoration of the fault blocks does not require rotation and produces small gaps and overlaps (Fig. 9). These characteristics attest to an approximately pure shear deformation.

5.2. Domino area

The domino areas are much larger than the conjugate areas. The northern area (Fig. 3) best exemplifies this style of deformation, having an abundance of large left-lateral faults (Fig. 5a and d). The central area (Fig. 4a) has some characteristics of a right-lateral domino domain.

5.2.1. Northern area

Left-lateral faults have a modal orientation of N050°E, which is a 20° clockwise rotation when compared with the modal orientation of left-lateral faults in the conjugate area. They have displacements of 10–80 m and compose 49% of the total trace

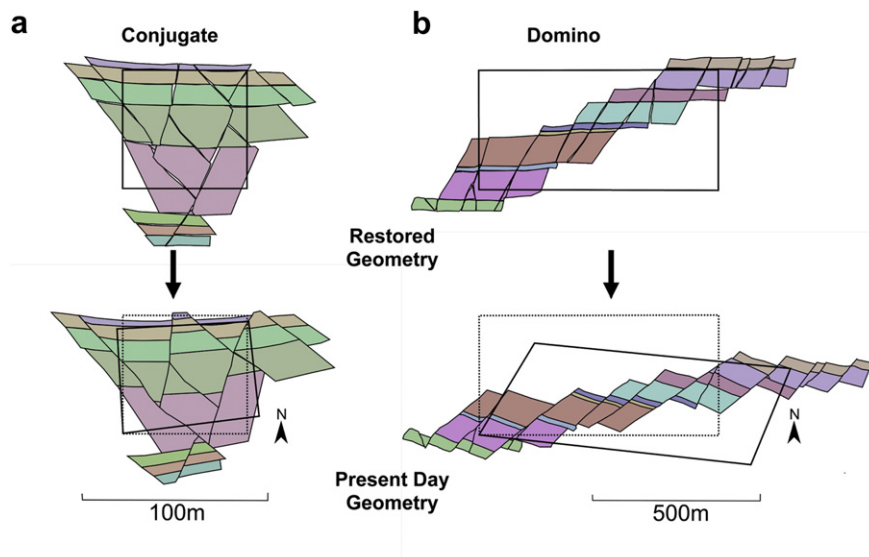


Fig. 9. Strain restoration diagrams a) the conjugate area (Fig. 4b) and b) the domino area (Fig. 3a).

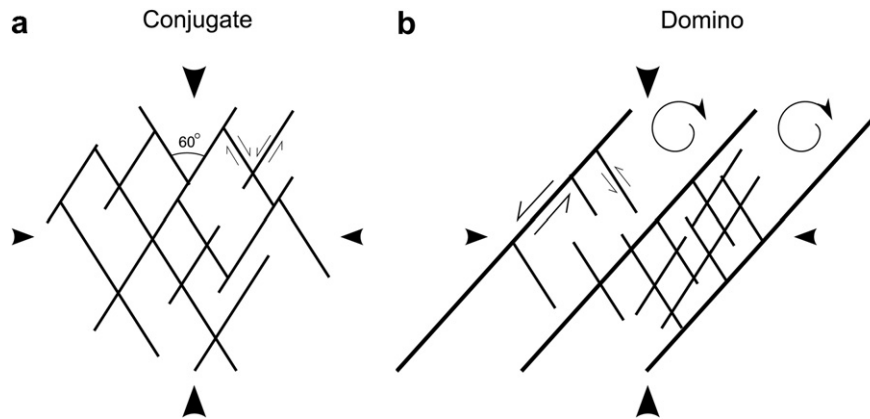


Fig. 10. Schematic diagram illustrating typical fault geometries: a) Conjugate fault network where faults have similar magnitudes and the maximum stress direction bisects the acute angle of intersection; b) Domino fault network with a dominant fault set and rotation of fault blocks. Arrows indicate far-field loading.

length for all faults in the subarea (Fig. 9b, Table 1) accounting for most of the displacement (Fig. 5d).

The northern domino area has approximately half the fault density (11 km^{-1}) of the conjugate area, but has about three times the extension (15.5%). The orientation of maximum extension is $\text{N}068^\circ\text{E}$. The strike of bedding between the dominant faults is $\text{N}110^\circ\text{E}$, which agrees well with the 20° clockwise rotation inferred from the fault rotation. The strain restoration illustrates the importance of block rotation of stratigraphy in the domino area, which accounts for the rotation of faults and bedding (Fig. 9).

5.2.2. Central area

Many features in the central (Fig. 4a) area fit a right-lateral domino model: trace length (Fig. 5c) and displacement (Fig. 5f) predominantly related to right-lateral faults. The right-lateral area has both antithetic and synthetic faults, compared to the well-developed antithetic faults between the main faults in the northern area. The fault density (19 km^{-1}) is intermediate between the northern domino area and the north central conjugate area, mainly due to the greater development of both sets of faults between the larger faults. This geometry shows that the internal fault block deformation of the right-lateral dominated areas is greater, with conjugate sets, forming small-displacement Y- and X-shaped fault intersections between large, widely spaced, right-lateral faults. The lack of rotation in the right-lateral domains could be due to greater internal deformation and the distance between large faults (Axen, 1988).

5.3. Damage area

The southern limit of the northern domino area occurs in the region surrounding the outcrop of the Rocknose Sandstone (Fig. 3b). This area is dominated by several large-displacement left-lateral faults with orientations of about $\text{N}030^\circ\text{E}$. Displacement along the main left-lateral faults is small where they curve with many small antithetic and synthetic faults, forming damage lenses, producing a large fault density of 39 km^{-1} . The complexity of the fault geometry in this area is enhanced by the development of synthetic splay faults and transfer faults across the lenses.

This damage area is situated between the well-developed conjugate and domino areas. It inherits some damage features related to the transition from domino to conjugate and the change from left-lateral to right-lateral dominant areas, and is related to

the change in fault dominance and kinematic behaviour (i.e. simple shear to pure shear).

6. Discussion

Displacement distribution profiles across individual faults within the network can be broadly categorised into two types:

- Conjugate interactions involving Y- and X-shaped intersections between faults with similar magnitudes. Similar kinematic characteristics have been found in other areas. Peacock (1991) described conjugate interactions between faults in Scotland where displacements on one fault are related to the other as the intersection point was approached. He also noted that conjugate intersections were associated with rapid loss of displacement at fault tips, much like examples in Fig. 7b and c.
- Antithetic and synthetic interactions, where large faults are linked to sets of smaller displacement faults with opposite and similar displacement senses, respectively. The smaller faults produce a series of systematic steps in the displacement profile of the larger fault. Kim et al. (2000) also found this change in displacement magnitudes for numerous antithetic fault interactions at Crackington Haven in North Cornwall, where small step-like decreases in displacement occurred like the main left-lateral fault in Fig. 7d.

The fault geometries, displacement distribution and the strain variation in the study area are heterogeneously developed throughout the whole strike-slip network. Conjugate areas lying between domino areas. This relationship has been observed in other types of fault systems where the dominant fault sets change. For example, McClay et al. (2002) described conjugate areas of normal faults in the east African rift system between areas dominated by east-dipping normal faults and west-dipping normal faults. Similarly, Fossen and Hesthammer (1998) described adjacent domino and conjugate (horst and graben) regions in the Gullfaks field in the Northern North Sea.

The strain distribution throughout the fault network at Westward Ho! indicates a more organised system with greater strains being accommodated by the development of domino regions that interact with each other. These domino regions have displacement and strain localized onto one of the fault sets with slip and rotation creating a change in orientation for the maximum extension.

Table 2
Characteristics of conjugate and domino regions.

	CONJUGATE	DOMINO
One fault set dominant	No	Yes
Symmetrical fault trend (displacement Weighted)	Yes	No
Equal displacement on both sets	Yes	No
Rotation of stratigraphy and faults	No	Yes

Where two domino regions with opposite dominant fault sets, interact with each other, a conjugate region forms.

6.1. *The existence of distinct conjugate and domino regions within the fault network allows a comparison between the two (summarized in Table 2)*

The conjugate area has symmetrical fault trends with similar trace-lengths and displacements on opposing fault sets. Evidence for significant rotation of either the faults or the stratigraphy is absent. Similar characteristics are found in other conjugate networks, for example the strike-slip fault networks in the Yilgarn Craton of western Australia (Vearncombe, 1998) and Nash Point in south Wales (Bourne and Willemse, 2001). The fault network map for Nash Point is very similar to that for the conjugate area at Westward Ho! (Figs. 10a and 4b), showing faults cross-cutting each other, forming conjugate fault intersections. Similar characteristics were also seen for conjugate normal faults (Nicol et al., 1995; Ferrill et al., 2000, 2009).

In contrast, the domino area contains a dominant fault set, with asymmetrical trace length and displacement weighted rose diagrams. Both the faults and bedding show a systematic rotation. Strike-slip movement in southern California also exhibits these domino characteristics with regions rotated clockwise and anti-clockwise depending on the dominant fault set. For example, the Mojave Desert Block has rotated anti-clockwise due to a dominance of right-lateral fault movement (Dokka and Travis, 1990), whereas the NE area of the Mojave Desert Block has accumulated a clockwise rotation due to the dominance of left-lateral faults (Luyendyk et al., 1980; Dokka and Travis, 1990). Furthermore, the original domino models observed by Wernicke and Burchfiel (1982) and Proffett (1977) in the Basin and Range region of the USA show similar characteristics for a normal fault system.

The applicability of these characteristics from the study area to other fault networks means that we can use them to identify whether a fault network is behaving in a domino or conjugate fashion (i.e. simple shear or pure shear, respectively) and whether it is kinematically homogeneous or heterogeneous. For the cases discussed here, the fault sets are at a high angle to layering which has a minimal affect on the resulting geometries. This means that the observations and characteristics are easily related to strike-slip and normal fault networks. However, this study cannot be as easily related to thrust regimes where layer-parallel detachment is usually more dominant and strongly influences fault geometry.

In this study, methods and observations, which have previously been used for individual faults, have been developed and applied to describe the geometry, kinematics and deformation of a fault network. This is an important step forward in fault analysis as faults rarely occur individually and without associated deformation. Hence, analysing faults on a network scale is vital to understanding the brittle deformation of the crust.

7. Conclusions

Detailed mapping on a well exposed wave-cut platform at Westward Ho!, north Devon is used to characterize a strike-slip

fault network. The fault network comprises NW-trending right-lateral faults and NE trending left-lateral faults. Geometric interactions between faults involve conjugate, antithetic and synthetic arrangements and include Y- and X-shaped intersection points, the former being most common.

Changes in the size and proportion of the fault sets within the fault network can be related to variations in bulk strain and kinematic behaviour, whilst preserving strain compatibility between different domains. Areas with domino fault geometries have:

- A dominant fault set with an asymmetry in (length \times displacement) weighted rose diagrams.
- A distinction between larger displacement, regularly spaced, faults of the dominant set and smaller antithetic faults in the intervening blocks. The smaller faults interact with the larger faults to produce changes in displacement along their lengths.
- Systematic rotation of both the dominant faults and bedding.

In contrast, areas with overall conjugate fault geometry have:

- Equal development of both sets of faults, and each have similar ranges of displacement.
- The interactions between faults typically produce abutting or cross-cutting relationships with displacement changes affecting both intersecting faults.
- Little or no rotation of the bedding.

Domino areas accumulated greater strains, with extensions of $\sim 15\%$ compared with $<5\%$ in conjugate areas. The higher strains are usually accommodated by a greater proportion of large-displacement faults and rotation of the maximum horizontal extension.

Restoration of fault displacement shows rotational strains in the domino areas and irrotational (pure shear) strain in the conjugate areas. Boundaries between these deformation domains are difficult to determine due to the limits of the exposures, but appear to be sub-parallel to bedding strike (i.e. E–W). Both the domino and conjugate areas have similar E–W extensions of $\sim 5\%$ and, hence, there is compatibility of strain across their boundaries. Damage zones can also be found between domains with lenses at fault bends and complex zones where faults die out against a large conjugate fault.

The techniques developed for the study area to analyse the fault patterns, interactions and resulting strains should be applicable to other fault networks. They can be used to analyse the deformation style, heterogeneity and strain/displacement localization within fault networks.

Acknowledgements

C.W. Nixon acknowledges financial support from NERC Case studentship (NE/H524922/1) with BP, and we are grateful to Steve Dee for his input into the project. The digital aerial photography was supplied by the Channel Coast Observatory. We thank Haakon Fossen, Alan Morris and Bill Dunne for their detailed and constructive comments, which have improved the resulting paper.

References

- Arthaud, F., Matte, P., 1977. Late Paleozoic strike-slip faulting in southern Europe and northern Africa: result of a right-lateral shear-zone between the Appalachians and the Urals. *Geological Society of America Bulletin* 88, 1305–1320.
- Axen, G.J., 1988. The geometry of planar domino-style normal faults above a dipping basal detachment. *Journal of Structural Geology* 10, 405–411.
- Aydin, A., Schultz, R.A., 1990. Effect of mechanical interaction on the development of strike-slip faults with echelon patterns. *Journal of Structural Geology* 12, 123–129.

- Badham, J.P.N., 1982. Strike-slip orogens – an explanation for the Hercynides. *Journal of the Geological Society* 139, 493–504.
- Barnes, R.P., Andrews, J.R., 1986. Upper Palaeozoic ophiolite generation and obduction in south Cornwall. *Journal of the Geological Society* 143, 117–124.
- Barnett, J.A.M., Mortimer, J., Rippon, J., Walsh, J.J., Watterson, J., 1987. Displacement geometry in the volume containing a single normal fault. *Bulletin of the American Association of Petroleum Geologists* 71, 925–937.
- Bourne, S.J., Willemsse, E.J.M., 2001. Elastic stress control on the pattern of tensile fracturing around a small fault network at Nash Point, UK. *Journal of Structural Geology* 23, 1753–1770.
- Cartwright, J.A., Trudgill, B.D., Mansfield, C.B., 1995. Fault growth by segment linkage: an explanation for scatter in maximum displacement and trace length data from the Canyonlands Grabens of SE Utah. *Journal of Structural Geology* 17, 1319–1326.
- Chadwick, R.A., 1993. Aspects of basin inversion in southern Britain. *Journal Geological Society of London* 150, 311–322.
- Childs, C., Watterson, J., Walsh, J.J., 1995. Fault overlap zones within developing normal fault systems. *Journal of the Geological Society* 152, 535–549.
- Coward, M.P., McClay, K.R., 1983. Thrust tectonics of S.Devon. *Journal Geological Society of London* 140, 215–228.
- Cox, S.J.D., Scholz, C.H., 1988. On the formation and growth of faults: an experimental study. *Journal of Structural Geology* 10, 413–430.
- Dearman, W.R., 1963. Wrench faulting in Cornwall and south Devon. *Proceedings Geological Association* 74, 265–287.
- Dokka, R.K., Travis, C.J., 1990. Late Cenozoic strike-slip faulting in the Mojave Desert, California. *Tectonics* 9, 311–340.
- Du, Y., Aydin, A., 1995. Shear fracture patterns and connectivity at geometric complexities along strike-slip faults. *Journal of Geophysical Research* 100, 18093–18102.
- Elliott, T., 1976. Upper Carboniferous sedimentary cycles produced by river dominated, elongate deltas. *Journal Geological Society of London* 132, 199–208.
- Ferrill, D.A., Morris, A.P., Stamatakos, J.A., Sims, D.W., 2000. Crossing conjugate normal fault. *American Association of Petroleum Geologist Bulletin* 84, 1543–1559.
- Ferrill, D.A., Morris, A.P., McGinnis, R.N., 2009. Crossing conjugate normal faults in field exposures and seismic data. *American Association of Petroleum Geologist Bulletin* 93, 1471–1488.
- Fossen, H., Hesthammer, J., 1998. Structural geology of the Gullfaks field, northern North Sea. In: Coward, M.P., Johnson, H., Daltaban, T.S. (Eds.), *Structural Geology in Reservoir Characterization*. Geological Society London Special Publication, 127, pp. 231–261.
- Freund, R., 1974. Kinematics of transform and transcurrent faults. *Tectonophysics* 21, 93–134.
- Higgs, R., Reading, H.G., Li, X., 1990. Upper Carboniferous Lacustrine and Deltaic Sedimentology, SW England: Westward Ho! and Bude. *British Sedimentological Research Group*.
- Holdsworth, R.E., 1989. The Start-Perranporth line: a Devonian terran boundary in the Variscan orogen on SW England. *Journal Geological Society of London* 146, 419–421.
- Horsfield, W.T., 1980. Contemporaneous movement along crossing conjugate normal faults. *Journal of Structural Geology* 5, 305–310.
- Huggins, P., Watterson, J., Walsh, J.J., Childs, C., 1995. Relay zone geometry and displacement transfer between normal faults recorded in coal-mine plans. *Journal of Structural Geology* 17, 1741–1755.
- Kelly, P.G., Sanderson, D.J., Peacock, D.C.P., 1998. Linkage and evolution of conjugate strike-slip fault zones in limestones of Somerset, Northumbria. *Journal of Structural Geology* 20, 1477–1493.
- Kim, Y.-S., Andrews, J.R., Sanderson, D.J., 2000. Damage zones around strike-slip fault systems and strike-slip evolution, Crackington Haven, southwest England. *Geoscience Journal* 4, 53–72.
- Kim, Y.-S., Andrews, J.R., Sanderson, D.J., 2001. Reactivated strike-slip faults: examples from north Cornwall. *Tectonophysics* 340, 173–194.
- Kim, Y.-S., Peacock, D.C.P., Sanderson, D.J., 2003. Strike-slip faults and damage zones at Marsalforn, Gozo Island, Malta. *Journal of Structural Geology* 25, 793–812.
- King, G.C.P., 1986. Speculations on the geometry of the initiation and termination processes of earthquake rupture and its relation tomorphology and geological structure. *Pura and Applied Geophysics* 124, 567–585.
- Lake, S.D., Karner, G.D., 1987. The structure and evolution of the Wessex Basin, southern England: an example of inversion tectonics. *Tectonophysics* 137, 347–378.
- Luyendyk, B.P., Kamerling, M.J., Terres, R., 1980. Geometric model for Neogene crustal rotations in southern California. *Geological Society of America Bulletin* 91, 211–217.
- McClay, K.R., Dooley, T., Whitehouse, P., Mills, M., 2002. 4-D evolution of rift systems: insights from scaled physical models. *American Association of Petroleum Geologists* 86, 935–959.
- Muraoka, H., Kamata, H., 1983. Displacement distribution along minor fault traces. *Journal of Structural Geology* 5, 483–495.
- Nicol, A., Walsh, J.J., Watterson, J., Bretan, P.G., 1995. Three-dimensional geometry and growth of conjugate normal faults. *Journal of Structural Geology* 17, 847–862.
- Nicol, A., Watterson, J., Walsh, J.J., Childs, C., 1996. The shapes, major axis orientations and displacement patterns of fault surfaces. *Journal of Structural Geology* 18, 235–248.
- Nur, A., Ron, H., Scotti, O., 1986. Fault mechanics and kinematics of block rotations. *Geology* 14, 746–749.
- Peacock, D.C.P., 1991. Displacements and segment linkage in strike-slip fault zones. *Journal of Structural Geology* 13, 1025–1035.
- Peacock, D.C.P., Sanderson, D.J., 1993. Estimating strain from fault slip using a line sample. *Journal of Structural Geology* 15, 1513–1516.
- Peacock, D.C.P., Sanderson, D.J., 1994. Geometry and development of relay ramps in normal fault systems. *American Association of Petroleum Geologists Bulletin* 78, 147–165.
- Peacock, D.C.P., Sanderson, D.J., 1995. Strike-slip relay ramps. *Journal of Structural Geology* 17, 1351–1360.
- Peacock, D.C.P., Sanderson, D.J., 1998. Deformation history and basin-controlling faults in the Mesozoic sedimentary rocks of the Somerset coast. *Proceedings Geological Association* 110, 41–52.
- Peacock, D.C.P., Anderson, M.W., Morris, A., Randall, D.E., 1998. Evidence for the importance of 'small' faults on block rotation. *Tectonophysics* 299, 1–13.
- Proffett, J.M., 1977. Cenozoic geology of the Yerington district, Nevada, and implications for the nature and origin of Basin and Range faulting. *Geological Society of America Bulletin* 88, 247–266.
- Ramsay, J.G., Huber, M.I., 1987. *Techniques of Modern Structural Geology*. In: *Folds and Fractures*, vol. 2. Academic Press, London.
- Sanderson, D.J., 1984. Structural Variation across the Northern Margin of the Variscides in NW Europe. In: *Journal Geological Society of London Special Publications*, 14, pp. 149–165.
- Sibson, R.H., 1989. Earthquake faulting as a structural process. *Journal of Structural Geology* 11, 1–14.
- Taylor, S.K., Bull, J.M., Lamarche, G., Barnes, P.M., 2004. Normal fault growth and linkage in the Whakatane graben, New Zealand, during the last 1.3 Myr. *Journal of Geophysical Research* 109, B02408.
- Vearncombe, J.R., 1998. Shear zones, fault networks, Archean gold. *Geology* 26, 855–858.
- Walker, T.G., 1970. Deposition of turbidites and agitated water siltstones: a study of the Upper Carboniferous Westward Ho! Formation, north Devon. *Proceedings Geological Association* 18, 43–67.
- Walsh, J.J., Watterson, J., 1987. Distributions of cumulative displacement and seismic slip on a single normal fault. *Journal of Structural Geology* 9, 1039–1046.
- Walsh, J.J., Watterson, J., 1988. Analysis and relationship between displacements and dimensions of faults. *Journal of Structural Geology* 10, 239–247.
- Wernicke, B., Burchfiel, B.C., 1982. Modes of extensional tectonics. *Journal of Structural Geology* 4, 105–115.
- Zhang, X., Sanderson, D.J., 2001. Evaluation of instability in fractured rock masses using numerical analysis methods: effects of fracture geometry and loading direction. *Journal of Geophysical Research* 106, 26671–26687.
- Zhao, G., Johnson, A.M., 1991. Sequential and incremental formation of conjugate sets of faults. *Journal of Structural Geology* 13, 887–895.